

LETTER TO THE EDITOR

# Discovery of $\text{HC}_3\text{O}^+$ in space: The chemistry of O-bearing species in TMC-1<sup>★</sup>

J. Cernicharo<sup>1</sup>, N. Marcelino<sup>1</sup>, M. Agúndez<sup>1</sup>, Y. Endo<sup>2</sup>, C. Cabezas<sup>1</sup>, C. Bermúdez<sup>1</sup>, B. Tercero<sup>3,4</sup>, and P. de Vicente<sup>4</sup>

<sup>1</sup> Grupo de Astrofísica Molecular, Instituto de Física Fundamental (IFF-CSIC), C/ Serrano 121, 28006 Madrid, Spain. e-mail : jose.cernicharo@csic.es

<sup>2</sup> Department of Applied Chemistry, Science Building II, National Chiao Tung University, 1001 Ta-Hsueh Rd., Hsinchu 30010, Taiwan

<sup>3</sup> Observatorio Astronómico Nacional (IGN), C/ Alfonso XII, 3, 28014, Madrid, Spain.

<sup>4</sup> Centro de Desarrollos Tecnológicos, Observatorio de Yebes (IGN), 19141 Yebes, Guadalajara, Spain.

Received; accepted

## ABSTRACT

Using the Yebes 40m and IRAM 30m radio telescopes, we detected a series of harmonically related lines with a rotational constant  $B_0=4460.590\pm 0.001$  MHz and a distortion constant  $D_0=0.511\pm 0.005$  kHz towards the cold dense core TMC-1. High-level-of-theory *ab initio* calculations indicate that the best possible candidate is protonated tricarbon monoxide,  $\text{HC}_3\text{O}^+$ . We have succeeded in producing this species in the laboratory and observed its  $J_a-J_b = 2-1$  and  $3-2$  rotational transitions. Hence, we report the discovery of  $\text{HC}_3\text{O}^+$  in space based on our observations, theoretical calculations, and laboratory experiments. We derive an abundance ratio  $N(\text{C}_3\text{O})/N(\text{HC}_3\text{O}^+)\sim 7$ . The high abundance of the protonated form of  $\text{C}_3\text{O}$  is due to the high proton affinity of the neutral species. The chemistry of O-bearing species is modelled, and predictions are compared to the derived abundances from our data for the most prominent O-bearing species in TMC-1.

**Key words.** Astrochemistry — ISM: molecules — ISM: individual (TMC-1) — line: identification — molecular data

## 1. Introduction

The cold dark core TMC-1 presents an interesting carbon-rich chemistry that leads to the formation of long neutral carbon-chain radicals and their anions (see Cernicharo et al. 2020a and references therein). Cyanopolyynes, which are stable molecules, are also particularly abundant in TMC-1 (see Cernicharo et al. 2020b and references therein). The chemistry of this peculiar object produces a large abundance of nearly saturated species, such as  $\text{CH}_3\text{CHCH}_2$ ; this species may mostly be a typical molecule of hot cores (Marcelino et al. 2007). The first polar benzenic ring,  $\text{C}_6\text{H}_5\text{CN}$  (McGuire et al. 2018), was also detected in this object, while benzene itself has only been detected to date towards post-asymptotic giant branch objects (Cernicharo et al. 2001). Hence, it has been a surprising result to see that, with an almost dominant carbon chemistry, O-bearing carbon chains such as  $\text{CCO}$  (Ohishi et al. 1991),  $\text{C}_3\text{O}$  (Matthews et al. 1984),  $\text{HC}_5\text{O}$ , and  $\text{HC}_7\text{O}$  are also produced in TMC-1 (Cordiner et al. 2017; McGuire et al. 2017). The formation path for  $\text{HC}_5\text{O}$  and  $\text{HC}_7\text{O}$  is still a mystery, as is the reason for the non-detection of  $\text{HC}_3\text{O}$ ,  $\text{HC}_4\text{O}$ , and  $\text{HC}_6\text{O}$  in the same cloud. The O-bearing carbon chain  $\text{HC}_2\text{O}$  has, however, been observed in cold dense clouds (Agúndez et al. 2015a).

<sup>★</sup> Based on observations carried out with the Yebes 40m telescope (projects 19A003 and 20A014) and the Institut de Radioastronomie Millimétrique (IRAM) 30m telescope. The 40m radio telescope at Yebes Observatory is operated by the Spanish Geographic Institute (IGN, Ministerio de Transportes, Movilidad y Agenda Urbana); IRAM is supported by INSU/CNRS (France), MPG (Germany), and IGN (Spain).

All long carbon chains containing oxygen that have been observed so far in interstellar clouds are neutral. Cationic species related to these oxygen-bearing neutral species are thought to play an important role in the synthesis of different neutral molecules in cold dense clouds. Moreover, it has been suggested that some of them may be sufficiently long-lived to be abundant (Petrie et al. 1993), although to date no such cation has been observed. In general, the abundance of polyatomic cations in cold interstellar clouds is relatively low because they react quickly with electrons. In addition to the widespread  $\text{HCO}^+$  and  $\text{N}_2\text{H}^+$ , the other polyatomic cations detected in cold interstellar clouds are  $\text{HCS}^+$  (Thaddeus et al. 1981),  $\text{HCNH}^+$  (Schilke et al. 1991),  $\text{HC}_3\text{NH}^+$  (Kawaguchi et al. 1994),  $\text{HCO}_2^+$  (Turner et al. 1999; Sakai et al. 2008),  $\text{NH}_3\text{D}^+$  (Cernicharo et al. 2013),  $\text{NCCNH}^+$  (Agúndez et al. 2015b),  $\text{H}_2\text{COH}^+$  (Bacmann et al. 2016),  $\text{H}_2\text{NCO}^+$  (Marcelino et al. 2018), and  $\text{HC}_5\text{NH}^+$  (Marcelino et al. 2020). These species are the protonated forms of abundant neutral species. The abundance ratio between a protonated molecule and its neutral counterpart,  $[\text{MH}^+]/[\text{M}]$ , is sensitive to the degree of ionization and thus to various physical parameters of the cloud, as well as the formation and destruction rates of the cation (Agúndez et al. 2015b). The protonated form is mainly formed by proton transfer to the neutral and destroyed by dissociative recombination with electrons. It is interesting to note that both chemical models and observations suggest a trend in which the abundance ratio  $[\text{MH}^+]/[\text{M}]$  increases with the increasing proton affinity of M (Agúndez et al. 2015b).

In this letter, we report the detection of four harmonically related lines that belong to a molecule with a  $^1\Sigma$  ground electronic state towards the cold dark core TMC-1. From microwave

**Table 1.** Observed line parameters for the new molecule in TMC-1.

$J_u-J_l$	$\nu_{obs}^a$ (MHz)	$\nu_o - \nu_c^b$ (kHz)	$\int T_A^* dv^c$ (mK km s <sup>-1</sup> )	$\Delta v^d$ (km s <sup>-1</sup> )	$T_A^*$ (mK)
4-3	35684.590	-0.6	9.1±0.5	0.63±0.03	13.8
5-4	44605.748	+4.4	10.7±0.6	0.45±0.03	22.5
10-9	89209.744	-11.3	6.4±1.0	0.44±0.09	13.8
11-10	98130.286	8.0	2.4±0.7	0.40±0.10	5.8

**Notes.**

(a) Observed frequencies adopting a  $v_{LSR}$  of 5.83 km s<sup>-1</sup> for TMC-1. The uncertainty is 10 kHz for all the lines.

(b) Observed minus calculated frequencies in kHz.

(c) Integrated line intensity in mK km s<sup>-1</sup>.

(d) Line width at half intensity derived by fitting a Gaussian line profile to the observed transitions (in km s<sup>-1</sup>).

laboratory experiments supported by *ab initio* calculations, we conclude that the carrier is HC<sub>3</sub>O<sup>+</sup>, the protonated form of C<sub>3</sub>O. We present a detailed observational study of the most relevant O-bearing species in this cloud and discuss these results in the context of state-of-the-art chemical models.

## 2. Observations

New receivers, built as part of the Nanocosmos project<sup>1</sup> and installed at the Yebes 40m radio telescope, were used for the observations of TMC-1. The Q-band receiver consists of two HEMT (high electron mobility transistor) cold amplifiers covering the 31.0-50.3 GHz band with horizontal and vertical polarizations. Receiver temperatures vary from 22 K at 32 GHz to 42 K at 50 GHz. The spectrometers are  $2 \times 8 \times 2.5$  GHz FFTs (Fast Fourier Transform) with a spectral resolution of 38.1 kHz, which provides full coverage of the Q-band in both polarizations. The main beam efficiency varies from 0.6 at 32 GHz to 0.43 at 50 GHz.

The observations leading to the line survey in Q-band towards TMC-1 ( $\alpha_{J2000} = 4^h41^m41.9^s$  and  $\delta_{J2000} = +25^\circ41'27.0''$ ) were performed over several sessions carried out between November 2019 and February 2020. The observing procedure was frequency switching with a frequency throw of 10 MHz. The nominal spectral resolution of 38.1 kHz was used for the final spectra. The sensitivity varies along the Q-band between 1 and 3 mK, which is a considerable improvement over previous line surveys in the 31-50 GHz frequency range (Kaifu et al. 2004).

The IRAM 30m data come from a line survey performed towards TMC-1 and B1. These observations have been described by Marcelino et al. (2007) and Cernicharo et al. (2013).

The antenna temperature intensity scale for the two telescopes used in this work was calibrated using two absorbers at different temperatures and the atmospheric transmission model ATM (Cernicharo 1985; Pardo et al. 2001). Calibration uncertainties were adopted to be 10%. All the data have been analysed using the GILDAS package<sup>2</sup>.

## 3. Results

Most of the weak lines found in our survey of TMC-1 can be assigned to known species and their isotopologues, and only a few remain unidentified (Marcelino et al., in preparation). As previously mentioned, the level of sensitivity has been increased by a factor of 5-10 with respect to previous line surveys performed with other telescopes at these frequencies (Kaifu et al. 2004).

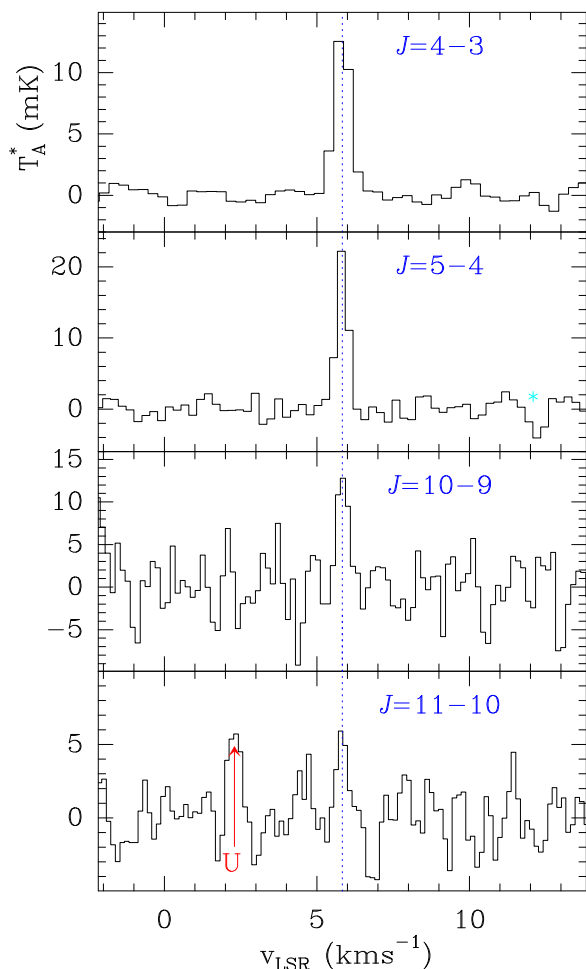


**Fig. 1.** Observed lines of the new molecule found in the 31-50 GHz domain towards TMC-1. The abscissa corresponds to the local standard of rest velocity in km s<sup>-1</sup>. Frequencies and intensities for the observed lines are given in Table 1. The ordinate is the antenna temperature corrected for atmospheric and telescope losses in mK. The  $J=11-10$  line is only detected at a  $3.5\sigma$  level. Spectral resolution is 38.1 kHz.

Frequencies for the unknown lines were derived by assuming a local standard of rest velocity of 5.83 km s<sup>-1</sup>, a value that was derived from the observed transitions of HC<sub>5</sub>N and its isotopologues in our line survey (Cernicharo et al. 2020a). Our new data towards TMC-1 have allowed us to detect the anions C<sub>3</sub>N<sup>-</sup> and C<sub>5</sub>N<sup>-</sup> (Cernicharo et al. 2020a), the cation HC<sub>5</sub>NH<sup>+</sup> (Marcelino et al. 2020), and the isomer HC<sub>4</sub>NC of HC<sub>5</sub>N (Cernicharo et al. 2020b), in addition to dozens of already known molecules.

The assignment of the observed features was done using the CDMS catalogue (Müller et al. 2005) and the MADEx code (Cernicharo 2012). Within the still unidentified features in our survey, we found two lines with a harmonic relation of 5:4 between them. The precision of this ratio is better than  $2 \times 10^{-5}$ . Taking into account the density of lines in TMC-1, the possibility that the harmonic relation between these two lines is the result of a fortuitous agreement is very small. Moreover, we explored our data at 3mm (Marcelino et al. 2007) and found two additional lines, the  $J=10-9$  line at 89209.749 MHz and the  $J=11-10$  transition at 98130.267 MHz. The frequency relation 4:5:10:11 between the four lines strongly suggests that the carrier is a linear molecule with a  $^1\Sigma$  ground electronic state. The observed lines are shown in Fig. 1, and the derived line parameters are given in Table 1.

<sup>1</sup> <https://nanocosmos.iff.csic.es/>

<sup>2</sup> <http://www.iram.fr/IRAMFR/GILDAS>

For a linear molecule in a  $^1\Sigma$  electronic state, the frequencies of its rotational transitions follow the standard expression  $\nu(J \rightarrow J-1) = 2B_0J - 4D_0J^3$ . By fitting the frequencies of the lines given in Table 1, we derive  $B_0 = 4460.58989 \pm 0.00096$  MHz and  $D_0 = 51.06 \pm 0.47$  Hz. The standard deviation of the fit is 10.3 kHz.

### 3.1. Potential carriers of the series of lines

An important piece of information to know when searching for the carrier of the lines is that the  $J=4-3$  line does not show any evidence of hyperfine splitting. A molecule with a terminal CN group will produce observable hyperfine splitting for its  $J=4-3$  transition. Hence, if the molecule contains a CN group, it should be an isocyano species (-NC terminal group). The typical hyperfine quadrupole splitting of a terminal NH group will also be unresolved for the  $J=4-3$  transition.

In TMC-1, only polyatomic molecules containing H, C, N, O, and S have been found so far. In order to evaluate the possible structure of the carrier, we can consider other species that have a similar rotational constant. Molecules such as HC<sub>3</sub>N ( $B_0 \sim 4549$  MHz), HC<sub>3</sub><sup>15</sup>N ( $B_0 \sim 4417$  MHz), C<sub>4</sub>H and C<sub>4</sub>D ( $B_0 \sim 4758$  MHz and 4416.4 MHz, respectively), the radical HCCCO (quasi-linear with  $(B+C)/2 \sim 4533$  MHz), NCCNH<sup>+</sup> ( $B_0 \sim 4438$  MHz), or H<sub>2</sub>C<sub>4</sub> ( $(B+C)/2 \sim 4466$  MHz) all provide a strong indication of the presence of four heavy atoms of C, N, and/or O, as well as a hydrogen or deuterium atom. Species containing sulphur, such as HCCS, HCCCS, or HNCSS, have rotational constants that are very different from the observed one.

In fact, despite being an asymmetrical molecule, the species that has a close match to our rotational constant is H<sub>2</sub>C<sub>4</sub>; its case has to be considered in detail as its series of  $J_{0,J}$  transitions are in good harmonic relation. Its lines are particularly prominent in TMC-1,  $T_A^* \sim 0.2$  K. Although the measured  $(B+C)/2$  value is  $\sim 6$  MHz above the observed one, its isotopologues H<sub>2</sub>C<sup>13</sup>CCC and H<sub>2</sub>CC<sup>13</sup>CC could have a slightly lower  $(B+C)/2$ . Its four <sup>13</sup>C isotopologues have been observed in the laboratory (McCarthy & Thaddeus 2002). Those corresponding to the second and third carbon in the molecule have  $(B+C)/2 \sim 4454.8$  and 4443.8 MHz, respectively. Hence, they do not match our  $B$  rotational constant. Moreover, taking into account the derived <sup>12</sup>C/<sup>13</sup>C abundance ratio in TMC-1 of  $\sim 90$  (Cernicharo et al. 2020b; Taniguchi et al. 2016), the expected intensities for the four <sup>13</sup>C isotopologues of H<sub>2</sub>C<sub>4</sub> are ten times weaker than the intensity of the observed lines (see Table 1 and Fig. 1). Finally, the rotational constant of the HDCCC isotopologue is smaller than that of our series of lines (Kim & Yamamoto 2005).

The cationic species derived from the protonation of CCCO, HCCCO<sup>+</sup>, was calculated by Botschwina (1989) to have a  $^1\Sigma$  ground electronic state with  $B_0 = 4454 \pm 10$  MHz. Recently, Thorwirth et al. (2020) performed high-level *ab initio* calculations and derived a rotational constant  $B_0 \sim 4460.4$  MHz, which matches our observed value very well. This species may be formed from the reaction of C<sub>3</sub>O with cations such as H<sub>3</sub><sup>+</sup> and HCO<sup>+</sup>. The proton affinity of C<sub>3</sub>O was calculated by Botschwina (1989) to be quite high,  $885 \pm 5$  kJ mol<sup>-1</sup>. From the observed trend of increasing protonated-to-neutral abundance ratios with increasing proton affinity (Agúndez et al. 2015b), a high abundance ratio HC<sub>3</sub>O<sup>+</sup>/C<sub>3</sub>O is expected.

Although HC<sub>3</sub>O<sup>+</sup> seems to be the best candidate, we have to explore other possible species derived from the isomers of NCCNH<sup>+</sup>, which also has a very close rotational constant of 4438.012 MHz (Gottlieb et al. 2000). In particular, CNCNH<sup>+</sup>,

**Table 2.** Rotational constants and electric dipole moments of potential candidates.

Molecule	$B_0$ (MHz)	$D$ (kHz)	$\mu^a$ (D)
New species <sup>b</sup>	4460.6	0.510	
HC <sub>3</sub> O <sup>+</sup> <sup>c</sup>	4460.5	0.469	3.41
HCNCN <sup>+</sup> <sup>d</sup>	4792.8	0.554	8.33
HNCNC <sup>+</sup> <sup>d</sup>	4899.1	0.511	3.96
HCNNC <sup>+</sup> <sup>d</sup>	5210.8	0.611	6.17
HCCNCH <sup>+</sup> <sup>d</sup>	4646.4	0.458	3.45
HNCCCH <sup>+</sup> <sup>d</sup>	4327.0	0.395	1.15
HCCCO <sup>-d</sup>	4246.8	0.311	0.31

#### Notes.

<sup>(a)</sup> Dipole moment calculated at the CCSD(T)-F12/cc-pCVTZ-F12 level of theory. <sup>(b)</sup> Values derived from the frequencies observed in TMC-1 (see Sect. 3). <sup>(c)</sup>  $B_0$  and  $D$  values scaled by the ratio Exp/Calc. of the corresponding parameter HC<sub>3</sub>N species. (See Table 3). <sup>(d)</sup> All the parameters for these species have been calculated at the CCSD(T)-F12/cc-pCVTZ-F12 level of theory. No corrections using scaling factors have been applied.

the protonated form of CNCN, which has also been found in space (Agúndez et al. 2018), could also be a good candidate. Other isomers with the proton on the terminal carbon atom are possible candidates as well (see Table 2). The protonated forms of the isomers of HC<sub>3</sub>N – HCCNCH<sup>+</sup> and HNCCCH<sup>+</sup> – could also have rotational constants around the observed value. The neutral isomers of cyanoacetylene have been observed towards TMC-1 and are abundant (see Cernicharo et al. 2020b and references therein), and the protonated form of HC<sub>3</sub>N has also been detected in this source (see Marcelino et al. 2020 and references therein).

### 3.2. Quantum chemical calculations and assignment to HC<sub>3</sub>O<sup>+</sup>

In order to obtain precise geometries and spectroscopic molecular parameters that help in the assignment of the observed lines, we carried out high-level *ab initio* calculations for all the species mentioned above. Table 2 shows the results from the geometry optimization calculations carried out at the CCSD(T)-F12/cc-pCVTZ-F12 level of theory (Raghavachari et al. 1989; Adler et al. 2007; Knizia et al. 2009; Hill et al. 2010a,b). This method has been proven to be suitable for accurately reproducing the molecular geometry of analogue molecules (Cernicharo et al. 2019; Marcelino et al. 2020). As can be seen, HCNCN<sup>+</sup>, HNCNC<sup>+</sup>, HCNNC<sup>+</sup>, and HCCNCH<sup>+</sup> all have rotational constants much larger than those derived from the frequencies observed in TMC-1. Hence, they can be excluded as carriers of the observed lines.

The  $B_e$  value obtained for HC<sub>3</sub>O<sup>+</sup> is 4457.383 MHz (see Table 3), which is very close to that derived for the new molecule. To obtain a more precise value for the rotational constant for HC<sub>3</sub>O<sup>+</sup>, we should estimate  $B_0$  by the zero-point vibrational contribution to the rotational constant and then calibrate this value using an experimental over theoretical ratio as scaling factor for analogue molecular species. At this point, two options are possible: C<sub>3</sub>O, which shares practically the same molecular structure, or HC<sub>3</sub>N, which is an isoelectronic species of HC<sub>3</sub>O<sup>+</sup>. Structural calculations at the CCSD(T)-F12/cc-pCVTZ-F12 level of theory give a  $B_e$  value for C<sub>3</sub>O of 4795.4 MHz, not very close to the experimental one of 4810.885 (33) (Brown et al. 1983). This discrepancy may be attributed to the floppy nature of

**Table 3.** Theoretical values for the spectroscopic parameters of  $\text{HC}_3\text{O}^+$  (all in MHz).

Parameter	$\text{HC}_3\text{N}$		$\text{HC}_3\text{O}^+$		
	Calc. <sup>a</sup>	Exp. <sup>b</sup>	Calc. <sup>a</sup>	Scaled. <sup>c</sup>	Scaled. <sup>d</sup>
$B_e$	4549.911		4457.383		
Vib-Rot. Corr.	4.899		1.630		
$B_0$	4544.215	4549.058558(40)	4455.753	4460.502	4460.443
$D \times 10^{-3}$	0.501	0.5442223(91)	0.432	0.469	0.471

**Notes.**

<sup>(a)</sup> This work; the  $B_0$  rotational constant has been estimated using the  $B_e$  value calculated at the CCSD(T)-F12/cc-pCVTZ-F12 level of theory and corrected with vibration-rotation interaction estimated at the MP2/cc-pVTZ level of theory. The centrifugal distortion constant has been calculated at the MP2/cc-pVTZ level of theory. <sup>(b)</sup> Thorwirth et al. (2000). <sup>(c)</sup> This work; scaled by the ratio Exp/Calc. of the corresponding parameter for the  $\text{HC}_3\text{N}$  species. <sup>(d)</sup> Thorwirth et al. (2020).

$\text{C}_3\text{O}$ , for which large zero-point vibrational contributions are expected. (Botschwina & Reisenauer 1991) For this reason,  $\text{C}_3\text{O}$  is not a good reference system to calibrate the  $\text{HC}_3\text{O}^+$  calculations, and, as such, we used  $\text{HC}_3\text{N}$  for this purpose. Table 3 shows the results for our calculations for  $\text{HC}_3\text{N}$  and those for  $\text{HC}_3\text{O}^+$ . After adding zero-point vibrational contribution to the  $B_e$  rotational constant and scaling by the ratio Experimental/Calculated for  $\text{HC}_3\text{N}$ , we obtained a  $B_0$  for  $\text{HC}_3\text{O}^+$  of 4460.502 MHz, which agrees perfectly with that derived from the TMC-1 lines. The centrifugal distortion value, obtained in the same manner but at the MP2/cc-pVTZ level of theory, is 0.469 kHz, which is compatible with that obtained from the fit of the lines. The results of our calculations are in agreement with those obtained by Thorwirth et al. (2020), which are also shown in Table 3. Finally, another potential candidate is  $\text{HC}_3\text{O}^-$ . However, our calculations indicate a rotational constant  $\sim 210$  MHz below the observed one and a very low permanent dipole moment (see Table 3). Hence, from the arguments provided in the previous section and our calculations, we conclude that the best candidate for the carrier of the observed lines is  $\text{HC}_3\text{O}^+$ .

### 3.3. Laboratory detection of $\text{HC}_3\text{O}^+$

In order to confirm our assignment of the astrophysical lines to  $\text{HC}_3\text{O}^+$ , we measured its microwave spectrum using a Balle-Flygare-type Fourier transform microwave (FTMW) spectrometer combined with a pulsed discharge nozzle (Endo et al. 1997; Cabezas et al. 2016), which has been used in the past to characterize other highly reactive molecules. The reactive transient species,  $\text{HC}_3\text{O}^+$ , was produced in a supersonic expansion by a pulsed electric discharge of a gas mixture of  $\text{C}_2\text{H}_2$  (0.15%), CO (0.8%), and  $\text{H}_2$  (1.0%) diluted in Ne, and with the application of a voltage of 800 V through the throat of the nozzle source. We searched for the  $J=2-1$  and  $3-2$  rotational transitions of  $\text{HC}_3\text{O}^+$ , predicting their frequencies from the rotational constants derived in TMC-1. These frequency regions were scanned and two lines were observed, within a few kilohertz of the predicted frequencies, at 17842.3387 and 26763.4749 MHz with an uncertainty of 5 kHz (see Fig. 2). The following experimental results confirm that these lines belong to a transient species: (i) they disappear in the absence of electric discharge and (ii) the lines disappear when one of the reactants ( $\text{C}_2\text{H}_2$  or CO) is removed from the gas mixture. No more lines at lower or higher frequencies ( $J_u - J_l = 1-0$  and  $4-3$ ) could be observed due to the spectrum weakness and the worse performance of the spectrometer at those frequencies.

We definitively conclude that the carrier of the observed lines is protonated tricarbon monoxide ( $\text{HC}_3\text{O}^+$ ). By merging the laboratory and astrophysical data, we derive

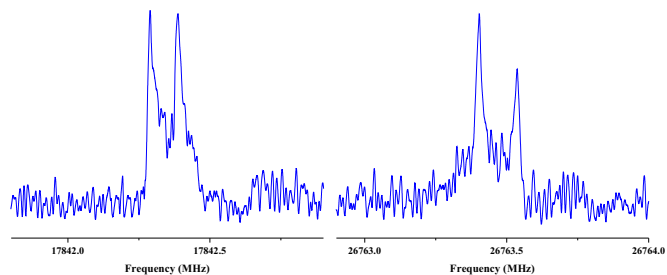


**Fig. 2.** FTMW spectra of  $\text{HC}_3\text{O}^+$  showing the 2-1 and 3-2 rotational transitions at 17842.3387 and 26763.4695 MHz, respectively. The spectra were achieved via 20000 shots of accumulation at a repetition rate of 10 Hz. The coaxial arrangement of the adiabatic expansion and the resonator axis produces an instrumental Doppler doubling. The resonance frequencies are calculated as the average of the two Doppler components.

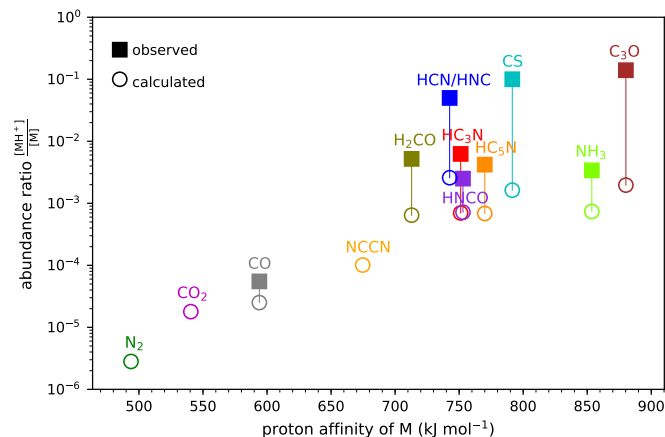


**Fig. 3.** Observed and calculated abundance ratios  $[\text{MH}^+]/[\text{M}]$  in cold dense clouds as a function of the proton affinity of the neutral M. They are based on Agúndez et al. (2015b), with updates for  $\text{H}_2\text{COH}^+$  from Bacmann et al. (2016), for  $\text{H}_2\text{NCO}^+$  from Marcelino et al. (2018), for  $\text{HC}_5\text{NH}^+$  from Marcelino et al. (2020), and for  $\text{HC}_3\text{O}^+$  from this study.

$$B_0 = 4460.58896 \pm 0.00057 \text{ MHz},$$

$$D_0 = 50.64 \pm 0.30 \text{ Hz},$$

which are the recommended constants for predicting the rotational spectrum of  $\text{HC}_3\text{O}^+$ . The standard deviation of the merged fit is 9.1 kHz. Frequency predictions have uncertainties  $\leq 10$  kHz for transitions below 100 GHz and  $\leq 100$  kHz for those in the range 100-180 GHz (see Table A.3).

## 4. Discussion

The detection of HC<sub>3</sub>O<sup>+</sup> in TMC-1 provides a further clue regarding the chemistry of protonated molecules in cold dense clouds. Agúndez et al. (2015b) find a trend in which the abundance ratio MH<sup>+</sup>/M increases with the increasing proton affinity of the neutral M. The C<sub>3</sub>O species has a very large proton affinity, ~885±5 kJ mol<sup>-1</sup> (Botschwina 1989). In fact, it is one of the largest proton affinities among abundant molecules in cold dark clouds. The observed abundance ratio  $N(\text{HC}_3\text{O}^+)/N(\text{C}_3\text{O})=0.14$  (see Appendix A and Table A.1) fits well with the expected value for a molecule with such a large proton affinity, according to the trend shown in Fig. 3. However, chemical model calculations similar to those presented in Agúndez et al. (2015b) predict an abundance ratio HC<sub>3</sub>O<sup>+</sup>/C<sub>3</sub>O of only  $2 \times 10^{-3}$  at steady state, which is almost two orders of magnitude below the observed value. Part of the discrepancy may stem from the fact that rate constants for the main reactions of the formation (proton transfer from H<sub>3</sub>O<sup>+</sup>, HCO<sup>+</sup>, and H<sub>3</sub><sup>+</sup>) and destruction (dissociative recombination with electrons) of HC<sub>3</sub>O<sup>+</sup> are not known, and thus chemical networks like UMIST RATE12 (McElroy et al. 2013) and KIDA kida.uva.2014 (Wakelam et al. 2015a) adopt estimates for them. These estimates, however, should not be drastically different from the real ones. In general, protonated-to-neutral abundance ratios are underestimated by chemical models, probably because chemical networks miss important formation routes for the cation (see Agúndez et al. 2015b and Fig. 3). In the case of HC<sub>3</sub>O<sup>+</sup>, additional formation routes may be provided by reactions of the ions C<sub>3</sub>H<sub>2</sub><sup>+</sup> and linear C<sub>3</sub>H<sub>3</sub><sup>+</sup> with O atoms, which is currently not considered in the aforementioned reaction networks. The reaction between C<sub>4</sub>H<sub>2</sub><sup>+</sup> and O atoms (e.g. Tenenbaum et al. 2006) is only an efficient route to HC<sub>3</sub>O<sup>+</sup> at very early times (< 10<sup>5</sup> yr), while reactions of C<sub>3</sub>H<sup>+</sup> with O<sub>2</sub>, H<sub>2</sub>O, and CO<sub>2</sub> (Herbst et al. 1984) are not a major route to HC<sub>3</sub>O<sup>+</sup> according to the chemical model. The sulphur analogue HC<sub>3</sub>S<sup>+</sup> is a good candidate for detection given that C<sub>3</sub>S has a very high proton affinity (933 kJ mol<sup>-1</sup>) and is around five times more abundant than C<sub>3</sub>O. We searched for it in our line survey using the *ab initio* calculations of Thorwirth et al. (2020) and derive an upper limit to its column density of  $3 \times 10^{11}$  cm<sup>-2</sup>, which implies an abundance ratio  $N(\text{HC}_3\text{S}^+)/N(\text{C}_3\text{S}) < 0.04$ . The lower MH<sup>+</sup>/M ratio of C<sub>3</sub>S compared to C<sub>3</sub>O probably stems from the fact that routes to HC<sub>3</sub>O<sup>+</sup> involving O atoms can be efficient because of the high abundance of neutral O atoms, while the sulphur analogous routes would be less efficient because atomic sulphur is expected to be preferably in ionized rather than neutral form.

In Table A.1, we present a comprehensive list of abundances derived from our data for O-bearing molecules in TMC-1. The chemistry of some of these species has already been discussed in detail, for example, in Agúndez et al. (2015a) and Wakelam et al. (2015b) for HCCO, in Loison et al. (2016) for the isomers *c*-H<sub>2</sub>C<sub>3</sub>O and HCCCHO, and in McGuire et al. (2017) and Cordiner et al. (2017) for HC<sub>5</sub>O and HC<sub>7</sub>O. These last O-bearing carbon chains deserve some discussion. They represent a new class of interstellar molecules and their chemistry is not yet well understood. Cordiner & Charnely (2012) proposed that HC<sub>*n*</sub>O molecules may directly form through reactions of hydrocarbon anions C<sub>*n*</sub>H<sup>-</sup> with O atoms in a process of associative electron detachment. This mechanism, however, overestimates the abundances of HC<sub>6</sub>O, C<sub>6</sub>O, and C<sub>7</sub>O by one to two orders of magnitude (Cordiner et al. 2017). McGuire et al. (2017) proposed that HC<sub>*n*</sub>O molecules could form through radiative association reactions of C<sub>*n*</sub>H<sub>2</sub><sup>+</sup> and C<sub>*n*</sub>H<sub>3</sub><sup>+</sup> ions with CO followed by disso-

ciative recombination with electrons. This mechanism explains the non-detection of HC<sub>6</sub>O in terms of a low reactivity between C<sub>5</sub>H<sub>2</sub><sup>+</sup> and CO (Adams et al. 1989), although it overestimates the abundance of HC<sub>4</sub>O by almost two orders of magnitude. The large abundance found for HC<sub>3</sub>O<sup>+</sup> suggests that reactions between hydrocarbon ions and atomic oxygen probably participate in the growth of these long O-bearing carbon chains.

*Acknowledgements.* The Spanish authors thank Ministerio de Ciencia e Innovación for funding support through projects AYA2016-75066-C2-1-P, PID2019-107115GB-C21. We also thank ERC for funding through grant ERC-2013-SyG-610256-NANOCOSMOS. MA and CB thanks MICIN for grants RyC-2014-16277 and FJCI-2016-27983, respectively. Y. Endo thanks Ministry of Science and Technology of Taiwan through grant MOST108-2113-M-009-25.

## References

- Adler, T. B., Knizia, G., Werner, H.-J., 2007 *J. Chem. Phys.* 127, 221106  
 Adams, N. G., Smith, D., Giles, K., & Herbst, E. 1989, *A&A*, 220, 269  
 Agúndez, M., Cernicharo, J., & Guélin, M. 2015a, *A&A*, 577, L5  
 Agúndez, M., Cernicharo, J., de Vicente, P., et al., 2015b, *A&A*, 579, L10  
 Agúndez, M., Marcelino, N., & Cernicharo, J. 2018, *ApJ*, 861, L22  
 Bacmann, A., García-García, E., & Faure, A. 2016, *A&A*, 588, L8  
 Botschwina, P., 1989, *J. Chem. Phys.*, 90, 4301  
 Botschwina, P., Reisenauer, H. P., 1991, *Chem. Phys. Lett.*, 183, 217.  
 Brown, R. D., Eastwood, F. W., Elmes, P. S., Godfrey, P. D., 1983 *J. Am. Chem. Soc.*, 105, 6496.  
 Cabezas, C., Guillemin, J.-C., Endo, Y. 2016, *J. Chem. Phys.*, 145, 184304.  
 Cernicharo, J. 1985, Internal IRAM report (Granada: IRAM)  
 Cernicharo, J., & Guélin, M. 1987, *A&A*, 176, 299  
 Cernicharo, J., Heras, A.M, Tielens, A.G.G.M., et al., 2001, *ApJ*, 546, L123  
 Cernicharo, J., 2012, in *ECLA 2011: Proc. of the European Conference on Laboratory Astrophysics*, EAS Publications Series, 2012, Ed.: C. Stehl, C. Joblin, & L. d'Hendecourt (Cambridge: Cambridge Univ. Press), 251; [https://nanocosmos.iff.csic.es/?page\\_id=1619](https://nanocosmos.iff.csic.es/?page_id=1619)  
 Cernicharo, J., Tercero, B., Fuente, A., et al. 2013, *ApJ*, 771, L10  
 Cernicharo, J., Cabezas, C., Pardo, J. R., et al., 2019, *A&A*, 630, L2  
 Cernicharo, J., et al., 2020a, *A&A*, 641, L9  
 Cernicharo, J., et al., 2020b, *A&A*, DOI:10.1051/0004-6361/202039274  
 Cordiner, M. A. & Chamley, S. B. 2012, *ApJ*, 749, 120  
 Cordiner, M. A., Chamley, S. B., Kisiel, Z., et al., 2017, *ApJ*, 850, 187  
 Endo, Y., Kohguchi, H., Ohshima, Y. 1994, *Faraday Discuss.*, 97, 341.  
 Fossé, D., Cernicharo, J., Gerin, M., Cox, P., 2001, *ApJ*, 552, 168  
 Gottlieb, C.A., Aponi, A.J., McCarthy, M.C., Thaddeus, P., 2000, *J. Chem. Phys.*, 113, 1910  
 Herbst, E., Smith, D., Adams, N.G., 1984, *A&A*, 138, L13  
 Hill, J. G., Mazumder, S., Peterson, K. A., 2010a, *J. Chem. Phys.*, 132, 054108  
 Hill, J. G., Peterson, K. A., 2010b, *Phys. Chem. Chem. Phys.*, 12, 10460  
 Kaifu, N., Ohishi, M., Kawaguchi, K., et al., 2004, *PASJ*, 56, 69  
 Kawaguchi, K., Kasai, Y., Ishikawa, S. et al., 1994, *ApJ*, 420, L95  
 Kim, E., Yamamoto, S., 2005, *J. Mol. Spectrosc.*, 233, 93  
 Knizia, G., Adler, T. B., Werner, H.-J., 2009 *J. Chem. Phys.* 130, 054104  
 Loison, J.-C., Agúndez, M., Marcelino, N., et al. 2016, *MNRAS*, 456, 4101  
 Matthews, H.E., Irvine, E., Friberg, F.M., et al., *Nature*, 310, 125  
 Marcelino, N., Cernicharo, J., Agúndez, M., et al. 2007, *ApJ*, 665, L127  
 Marcelino, N., Agúndez, M., Cernicharo, J., et al. 2018, *A&A*, 612, L10  
 Marcelino, N., et al., 2020, *A&A*, DOI:10.1051/0004-6361/202039251  
 McCarthy, M.C., Thaddeus, P., 2002, *J. Mol. Spectrosc.*, 211, 235  
 McElroy, D., Walsh, C., Markwick, A. J., et al. 2013, *A&A*, 550, A36  
 McGuire, B.A., Burkhardt, M., Shingledecker, C.N., et al., 2017, *ApJ*, 843, L28  
 McGuire, B.A., Burkhardt, M., Kalenskii, S., et al., 2018, *Science*, 359, 202  
 Müller, H.S.P., Schlöder, F., Stutzki, J., Winnewisser, G., 2005, *J. Mol. Struct.*, 742, 215  
 Ohishi, M., Suzuki, H., Ishikawa, S.-I., et al., 1991, *ApJ*, 380, L39  
 Pardo, J. R., Cernicharo, J., Serabyn, E. 2001, *IEEE Trans. Antennas and Propagation*, 49, 12  
 Petrie, S., Bettens, R. P. A., Freeman, C. G., & McEwan, M. J. 1993, *MNRAS*, 264, 862  
 Raghavachari, K., Trucks, G. W., Pople, J. A., Head-Gordon, M., 1989, *Chem. Phys. Lett.*, 157, 479  
 Sakai, N., Sakai, T., Aikawa, Y., Yamamoto, S. 2008, *ApJ*, 675, L89  
 Schilke, P., Walmsley, C. M., Millar, T. J., Henkel, C. 1991, *A&A*, 247, 487  
 Taniguchi, K., Ozeki, H., Saito, M., et al., 2016, *ApJ*, 817, 147  
 Tenenbaum, E.D., Aponi, A.J., Ziurys, L.M., et al., 2006, *ApJ*, 649, L17  
 Thaddeus, P., Guélin, M., Linke, R. A. 1981, *ApJ*, 246, L41  
 Thorwirth, S., Müller, H. S. P. Winnewisser, G., 2000, *J. Mol. Spectrosc.*, 204, 133  
 Thorwirth, S., Harding, M.E., Asvany, O., et al., 2020, *Mol. Phys.*, in press  
 Turner, B. E., Terzieva, R., Herbst, E. 1999, *ApJ*, 518, 699  
 Wakelam, V., Loison, J.-C., Herbst, E., et al. 2015a, *ApJS*, 217, 20  
 Wakelam, V., Loison, J.-C., Hickson, K. M., & Ruaud, M. 2015b, *MNRAS*, 453, L48



**Table A.1.** Column densities for relevant O-bearing species in TMC-1.

Molecule	$N^a$	$X^b$	$N(\text{CH}_3\text{OH})/N$	
HCCCO <sup>+</sup>	$2.1(2)\times 10^{11}$	$2.1\times 10^{-11}$	229	
HOCO <sup>+</sup>	$4.0(2)\times 10^{11}$	$4.0\times 10^{-11}$	120	
H <sub>2</sub> COH <sup>+</sup>	$\leq 3.0\times 10^{11}$	$\leq 3.0\times 10^{-11}$	$\geq 160$	
H <sub>2</sub> NCO <sup>+</sup>	$\leq 4.0\times 10^{10}$	$\leq 4.0\times 10^{-12}$	$\geq 1200$	
HNCO	$1.3(1)\times 10^{13}$	$1.3\times 10^{-9}$	3.7	
HCNO	$7.0(3)\times 10^{10}$	$7.0\times 10^{-12}$	686	
HOCN	$1.1(2)\times 10^{11}$	$1.1\times 10^{-11}$	437	
CH <sub>3</sub> OH	$4.8(3)\times 10^{13}$	$4.8\times 10^{-9}$	1	A + E
CCO	$1.5(3)\times 10^{12}$	$1.5\times 10^{-10}$	32	
CCCO	$1.5(2)\times 10^{12}$	$1.5\times 10^{-10}$	32	
CCCCO	$\leq 1.2\times 10^{11}$	$\leq 1.2\times 10^{-11}$	$\geq 400$	
CCCCCO	$\leq 4.0\times 10^{10}$	$\leq 4.0\times 10^{-12}$	$\geq 1200$	
HCOOH	$1.4(2)\times 10^{12}$	$1.4\times 10^{-10}$	34	
HCCO	$1.0(2)\times 10^{12}$	$1.0\times 10^{-10}$	48	
HCCCO	$\leq 2.0\times 10^{11}$	$\leq 2.0\times 10^{-11}$	$\geq 240$	
HCCCOO	$\leq 3.0\times 10^{11}$	$\leq 3.0\times 10^{-11}$	$\geq 160$	
HCCCCCO	$1.8(2)\times 10^{12}$	$1.8\times 10^{-10}$	27	
HCCCCCOO	$\leq 7.0\times 10^{11}$	$\leq 7.0\times 10^{-11}$	$\geq 59$	
HCCCCCCCO	$\leq 9.0\times 10^{11}$	$\leq 9.0\times 10^{-11}$	$\geq 53$	
H <sub>2</sub> CCO	$1.4(2)\times 10^{13}$	$1.4\times 10^{-9}$	3.4	o + p
H <sub>2</sub> CCCO	$\leq 1.1\times 10^{11}$	$\leq 1.1\times 10^{-11}$	$\geq 436$	
c-H <sub>2</sub> C <sub>3</sub> O	$4.0(2)\times 10^{11}$	$4.0\times 10^{-11}$	120	o + p
HCCCHO	$2.0(2)\times 10^{12}$	$2.0\times 10^{-10}$	240	
H <sub>2</sub> CCCOO	$\leq 1.2\times 10^{11}$	$\leq 1.2\times 10^{-11}$	$\geq 400$	o
CH <sub>3</sub> CHO	$3.5(2)\times 10^{12}$	$3.5\times 10^{-10}$	14	A + E
NH <sub>2</sub> CHO	$\leq 5.0\times 10^{10}$	$\leq 5.0\times 10^{-12}$	$\geq 960$	
HCCCCOH	$\leq 1.0\times 10^{11}$	$\leq 1.0\times 10^{-11}$	$\geq 480$	

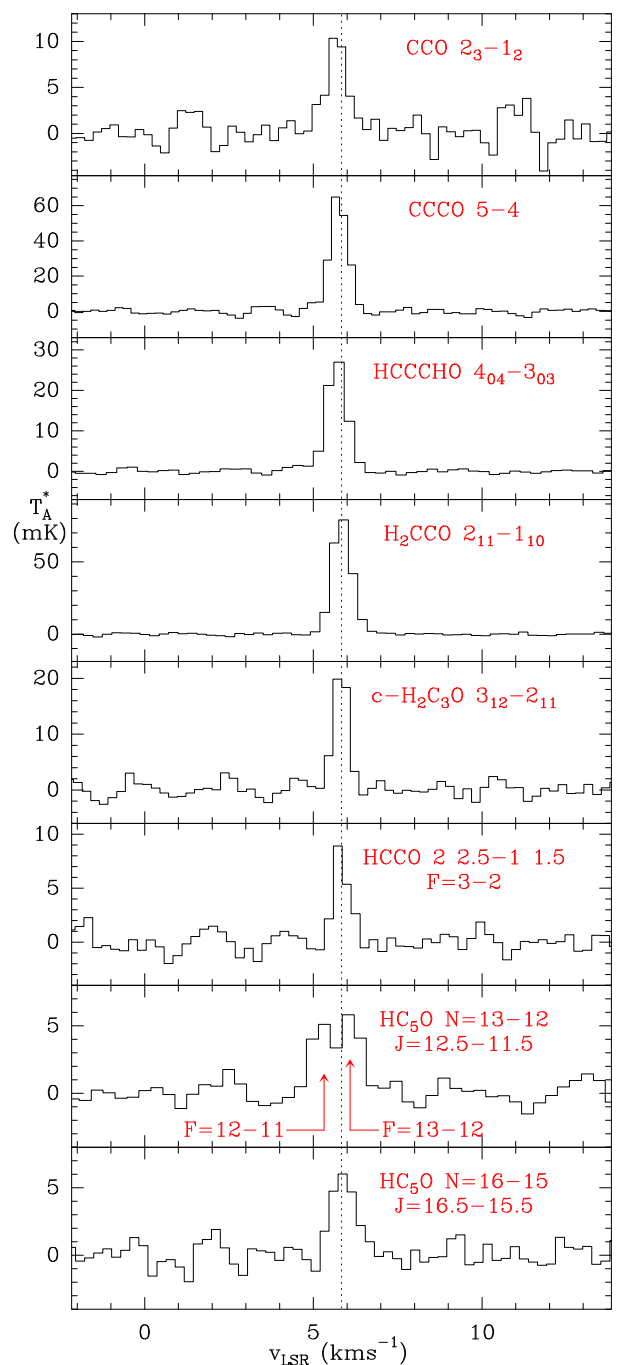
**Notes.**
<sup>(a)</sup> Column density in cm<sup>-2</sup>. Upper limits correspond to 3 $\sigma$  values.

<sup>(b)</sup> Relative abundance to H<sub>2</sub> assuming a total column density of molecular hydrogen of 10<sup>22</sup> cm<sup>-2</sup> (Cernicharo & Guélin 1987).

**Appendix A: Observational data for O-bearing species in TMC1**

In order to study the chemistry of O-bearing species in TMC-1, we explored the lines arising from these species in our line survey. The derived line parameters are given in Table A.2, and some selected lines are shown in Fig. A.1. Line parameters were derived by fitting a Gaussian line profile to the observed features. Rest frequencies were adopted from the MADEx code (Cernicharo 2012). In order to derive column densities, we assumed that all molecular species are thermalized at a temperature of 10 K. Main beam efficiency (see Sect. 2) and source dilution in the beam were applied to all the observations. For the source dilution, we assumed a source radius of 40'' (Fossé et al. 2001), that is to say, the source practically fills the main beam of the telescope at all observed frequencies. The derived column densities of detected O-bearing species in our survey were obtained using the MADEx code and are given in Table A.1. The 1 $\sigma$  sensitivity of the survey is ~0.6-0.7 mK and 0.7-2.0 mK below and above 40 GHz, respectively. Hence, the data allow us to derive very sensitive 3 $\sigma$  upper limits for the column density of many O-bearing species, which are given in Table A.1. It is worth noting that although many lines of HC<sub>5</sub>O are detected in our survey, only upper limits have been obtained for HC<sub>7</sub>O lines, which has been reported previously by McGuire et al. (2017) and Cordiner et al. (2017) using line stacking.

Table A.3 provides the frequencies, uncertainties, upper energy levels, Einstein coefficients, and degeneracies for transitions up to  $J=30-29$ . This information is provided with the intent of facilitating the search for HC<sub>3</sub>O<sup>+</sup> in other sources and with other instruments.


**Fig. A.1.** Selected lines of O-bearing species observed towards TMC1 in the 31-50 GHz domain. The abscissa corresponds to the local standard of rest velocity in km s<sup>-1</sup>. Frequencies and intensities for the observed lines are given in Table A.2. The ordinate is the antenna temperature corrected for atmospheric and telescope losses in mK. Spectral resolution is 38.1 kHz.

**Table A.2.** Derived line parameters for O-bearing species in TMC-1.

Molecule	Transition	$\nu_{rest}^a$ (MHz)	$\int T_A^* dv^b$ (mK km s <sup>-1</sup> )	$v_{LSR}^c$ (km s <sup>-1</sup> )	$\Delta v^d$ (km s <sup>-1</sup> )	$T_A^* e$ (mK)
CCO	1 <sub>1</sub> -0 <sub>1</sub>	32623.449±0.007	5.1±0.7	5.57(05)	1.09(13)	4.5
CCO	2 <sub>1</sub> -1 <sub>1</sub>	32738.613±0.005	1.6±0.7	6.33(18)	1.46(34)	1.0
CCO	2 <sub>3</sub> -1 <sub>2</sub>	45826.734±0.002	8.1±0.9	5.69(04)	0.73(11)	10.0
CCO	2 <sub>2</sub> -1 <sub>1</sub>	46182.187±0.002	2.5±1.0	5.73(17)	0.89(31)	2.7
CCCO	4-3	38486.891±0.001	43.5±1.0	5.74(01)	0.63(07)	64.5
CCCO	5-4	48108.474±0.001	44.2±1.0	5.75(01)	0.63(14)	66.4
HNCO	2 <sub>02</sub> -1 <sub>01</sub> 1-1	43962.007±0.030	20.1±1.0	5.76(01)	0.62(02)	35.1
HNCO	2 <sub>02</sub> -1 <sub>01</sub> 1-2	43962.641±0.006				≤2.7
HNCO	2 <sub>02</sub> -1 <sub>01</sub> 3-2	43963.000±0.030	178.8±1.0	5.76(01)	0.68(01)	247.8
HNCO	2 <sub>02</sub> -1 <sub>01</sub> 2-1	43963.000±0.030				
HNCO	2 <sub>02</sub> -1 <sub>01</sub> 1-0	43963.626±0.030	26.1±2.0	6.35(02)	0.60(04)	41.2
HNCO	2 <sub>02</sub> -1 <sub>01</sub> 2-2	43963.626±0.030	22.9±2.0	5.66(03)	0.64(05)	33.6
HCNO	2-1	45876.069±0.002	7.1±1.0	5.79(08)	0.98(16)	6.9
HOCN	2 <sub>02</sub> -1 <sub>01</sub>	41950.836±0.001	13.6±1.0	5.55(02)	0.82(03)	15.6
HCOOH	2 <sub>12</sub> -1 <sub>11</sub>	43303.705±0.001	3.4±0.5	6.10(09)	0.61(10)	5.2
HCOOH	2 <sub>02</sub> -1 <sub>01</sub>	44911.734±0.001	6.7±0.5	5.82(05)	0.79(10)	7.9
HCOOH	2 <sub>11</sub> -1 <sub>10</sub>	46581.220±0.001	2.1±0.5	5.95(14)	0.70(22)	2.8
HCCCHO	4 <sub>14</sub> -3 <sub>13</sub>	36648.266±0.006	7.4±0.5	5.76(02)	0.78(05)	9.0
HCCCHO	4 <sub>04</sub> -3 <sub>03</sub>	37290.136±0.006	21.0±0.5	5.64(01)	0.70(02)	28.1
HCCCHO	4 <sub>13</sub> -3 <sub>12</sub>	37954.572±0.006	10.4±0.5	5.59(01)	0.74(04)	13.2
HCCCHO	5 <sub>15</sub> -4 <sub>14</sub>	45807.708±0.007	3.5±0.7	5.73(05)	0.46(10)	7.3
HCCCHO	5 <sub>05</sub> -4 <sub>04</sub>	46602.868±0.007	25.5±0.5	5.64(01)	0.65(02)	3.6
HCCCHO	5 <sub>14</sub> -4 <sub>13</sub>	47440.427±0.007	6.0±0.7	5.61(04)	0.55(09)	10.3
A-CH <sub>3</sub> CHO	4 <sub>04</sub> -3 <sub>13</sub>	32709.214±0.002				≤1.8
A-CH <sub>3</sub> CHO	2 <sub>12</sub> -1 <sub>11</sub>	37464.204±0.001	12.1±1.0	5.84(02)	0.91(06)	12.5
A-CH <sub>3</sub> CHO	2 <sub>02</sub> -1 <sub>01</sub>	38512.079±0.001	31.3±0.6	5.85(01)	0.82(01)	35.7
A-CH <sub>3</sub> CHO	2 <sub>11</sub> -1 <sub>10</sub>	39594.289±0.001	14.0±1.0	5.83(02)	0.79(05)	16.6
A-CH <sub>3</sub> CHO	1 <sub>10</sub> -1 <sub>01</sub>	47820.620±0.002	4.3±0.6	5.76(08)	0.65(13)	6.1
A-CH <sub>3</sub> CHO	2 <sub>11</sub> -2 <sub>02</sub>	48902.831±0.002	4.0±0.6	5.76(07)	0.66(13)	5.6
E-CH <sub>3</sub> CHO	4 <sub>+04</sub> -3 <sub>-13</sub>	33236.468±0.002				≤2.0
E-CH <sub>3</sub> CHO	2 <sub>-12</sub> -1 <sub>+10</sub>	35837.312±0.003	1.3±0.6	5.89(09)	0.62(20)	2.0
E-CH <sub>3</sub> CHO	2 <sub>-12</sub> -1 <sub>-11</sub>	37686.932±0.002	9.7±1.0	5.88(02)	0.75(05)	12.1
E-CH <sub>3</sub> CHO	2 <sub>+02</sub> -1 <sub>+01</sub>	38506.035±0.001	33.7±1.0	5.85(01)	0.82(01)	38.5
E-CH <sub>3</sub> CHO	2 <sub>+11</sub> -1 <sub>+10</sub>	39362.537±0.002	13.8±1.0	5.82(02)	0.84(04)	15.4
E-CH <sub>3</sub> CHO	2 <sub>+11</sub> -1 <sub>-11</sub>	41212.157±0.003	2.5±0.8	6.07(09)	0.83(16)	2.8
E-CH <sub>3</sub> CHO	1 <sub>-11</sub> -1 <sub>+01</sub>	45897.347±0.003				≤3.0
E-CH <sub>3</sub> CHO	1 <sub>+10</sub> -1 <sub>+01</sub>	47746.968±0.002	2.5±0.8	6.17(22)	0.82(23)	2.8
E-CH <sub>3</sub> CHO	2 <sub>+11</sub> -2 <sub>+02</sub>	48603.469±0.002	6.8±1.0	5.88(05)	0.75(11)	8.6
o-H <sub>2</sub> CCO	2 <sub>12</sub> -1 <sub>11</sub>	40039.017±0.001	57.8±0.7	5.77(01)	0.68(01)	79.5
o-H <sub>2</sub> CCO	2 <sub>11</sub> -1 <sub>10</sub>	40793.842±0.001	59.4±0.7	5.79(01)	0.68(01)	81.9
p-H <sub>2</sub> CCO	2 <sub>02</sub> -1 <sub>01</sub>	40417.950±0.001	37.9±0.7	5.78(01)	0.64(02)	55.9
o-c-H <sub>2</sub> C <sub>3</sub> O	3 <sub>13</sub> -2 <sub>12</sub>	39956.733±0.004	14.9±0.8	5.81(01)	0.65(03)	21.5
o-c-H <sub>2</sub> C <sub>3</sub> O	3 <sub>12</sub> -2 <sub>11</sub>	44587.397±0.004	12.4±0.8	5.82(01)	0.51(03)	22.8
p-c-H <sub>2</sub> C <sub>3</sub> O	3 <sub>03</sub> -2 <sub>02</sub>	42031.939±0.004	6.4±0.8	5.78(03)	0.68(07)	8.9
p-c-H <sub>2</sub> C <sub>3</sub> O	3 <sub>22</sub> -2 <sub>21</sub>	42316.187±0.003	1.7±0.7	5.78(02)	0.27(10)	6.0
p-c-H <sub>2</sub> C <sub>3</sub> O	3 <sub>21</sub> -2 <sub>20</sub>	42601.246±0.003	2.4±0.7	5.94(03)	0.48(09)	4.6
HCCO	2,2.5-1,1.5 F=3-2	43317.673±0.006	4.9±0.8	5.80(03)	0.51(08)	8.9
HCCO	2,2.5-1,1.5 F=2-1	43321.150±0.006	3.8±0.8	5.70(05)	0.67(15)	5.4
HCCO	2,1.5-1,0.5 F=2-1	43329.543±0.006	3.8±0.8	5.67(06)	0.64(15)	5.5
HCCO	2,1.5-1,0.5 F=1-0	43335.462±0.004	4.2±0.8	5.69(08)	0.97(17)	4.1
HC <sub>5</sub> O	13 1 12.5-12 -1 11.5 13-12	32267.964±0.002	3.7±0.9	5.52(06)	0.63(09)	5.6
HC <sub>5</sub> O	13 1 12.5-12 -1 11.5 12-11	32268.049±0.002	4.8±1.0	5.65(07)	0.73(15)	6.0
HC <sub>5</sub> O	13 -1 12.5-12 1 11.5 13-12	32271.760±0.002	2.7±1.0	5.59(08)	0.62(14)	3.9
HC <sub>5</sub> O	13 -1 12.5-12 1 11.5 12-11	32271.848±0.002	4.3±1.0	5.62(06)	0.76(15)	5.4
HC <sub>5</sub> O	14 -1 13.5-13 1 12.5 14-13	34849.461±0.002	1.9±0.7	5.58(02)	0.33(16)	5.0
HC <sub>5</sub> O	14 -1 13.5-13 1 12.5 13-12	34849.540±0.002	4.5±1.0	5.67(03)	0.81(08)	5.3
HC <sub>5</sub> O	14 1 13.5-13 -1 12.5 14-13	34853.387±0.002	4.5±1.0	5.69(17)	0.74(14)	5.7
HC <sub>5</sub> O	14 1 13.5-13 -1 12.5 13-12	34853.469±0.002	3.1±0.9	5.63(14)	0.54(16)	5.4
HC <sub>5</sub> O	15 1 14.5-14 -1 13.5 15-14 <sup>f</sup>	37430.982±0.003	6.3±1.0	5.79(03)	0.93(05)	6.4

Table A.2. continued.

Molecule	Transition	$\nu_{rest}^a$ (MHz)	$\int T_A^* dv^b$ (mK km s <sup>-1</sup> )	$v_{LSR}^c$ (km s <sup>-1</sup> )	$\Delta v^d$ (km s <sup>-1</sup> )	$T_A^*$ (mK)
HC <sub>5</sub> O	15 -1 14.5-14 1 13.5 15-14 <sup>f</sup>	37435.050±0.003	6.2±1.0	5.79(04)	0.99(09)	5.9
HC <sub>5</sub> O	15 -1 15.5-15 1 14.5 16-15 <sup>f</sup>	40012.451±0.004	5.3±1.0	5.80(06)	1.00(12)	4.9
HC <sub>5</sub> O	15 1 15.5-15 -1 14.5 16-15 <sup>f</sup>	40016.668±0.004	7.1±1.0	5.86(04)	1.02(10)	6.5
HC <sub>5</sub> O	16 1 16.5-15 -1 15.5 17-16 <sup>f</sup>	42593.906±0.004	5.2±1.0	5.70(05)	0.77(09)	6.3
HC <sub>5</sub> O	16 -1 16.5-15 1 15.5 17-16 <sup>f</sup>	42598.284±0.004	5.4±1.0	5.89(04)	0.82(09)	6.2
HC <sub>5</sub> O	17 -1 17.5-16 1 16.5 18-17 <sup>f</sup>	45175.346±0.005	5.4±1.0	5.75(11)	1.05(19)	4.8
HC <sub>5</sub> O	17 1 17.5-16 -1 16.5 18-17 <sup>f</sup>	45179.895±0.005	6.3±1.0	5.80(08)	1.06(17)	5.6
HC <sub>5</sub> O	18 1 18.5-17 -1 17.5 19-18 <sup>f</sup>	47756.772±0.007				≤5.1
HC <sub>5</sub> O	18 -1 18.5-17 1 17.5 19-18 <sup>f</sup>	47761.501±0.007				≤5.1

**Notes.**

<sup>(a)</sup> Rest frequencies and uncertainties from MADEX (Cernicharo 2012).

<sup>(b)</sup> Integrated line intensity in mK kms<sup>-1</sup>.

<sup>(c)</sup> Local standard of rest velocity of the observed emission kms<sup>-1</sup>.

<sup>(d)</sup> Line width at half intensity derived by fitting a Gaussian line profile to the observed transitions (in kms<sup>-1</sup>).

<sup>(e)</sup> Upper limits to the antenna temperature correspond to 3 $\sigma$  values.

<sup>(f)</sup> Average of two hyperfine components.



**Table A.3.** Predicted frequencies of HC<sub>3</sub>O<sup>+</sup>.

Transition	$\nu$ (MHz)	$E_{up}$ (K)	$A_{ij}$ (s <sup>-1</sup> )	$S_{ij}$	$g_u$
1→0	8921.175±0.001	0.4	2.928 10 <sup>-08</sup>	1	3
2→1	17842.338±0.003	1.3	2.810 10 <sup>-07</sup>	2	5
3→2	26763.477±0.004	2.6	1.016 10 <sup>-06</sup>	3	7
4→3	35684.579±0.005	4.3	2.498 10 <sup>-06</sup>	4	9
5→4	44605.633±0.006	6.4	4.990 10 <sup>-06</sup>	5	11
6→5	53526.627±0.006	9.0	8.756 10 <sup>-06</sup>	6	13
7→6	62447.547±0.006	12.0	1.406 10 <sup>-05</sup>	7	15
8→7	71368.383±0.006	15.4	2.116 10 <sup>-05</sup>	8	17
9→8	80289.124±0.006	19.3	3.033 10 <sup>-05</sup>	9	19
10→9	89209.754±0.008	23.5	4.182 10 <sup>-05</sup>	10	21
11→10	98130.263±0.010	28.3	5.590 10 <sup>-05</sup>	11	23
12→11	107050.638±0.014	33.4	7.284 10 <sup>-05</sup>	12	25
13→12	115970.868±0.020	39.0	9.290 10 <sup>-05</sup>	13	27
14→13	124890.942±0.027	45.0	1.163 10 <sup>-04</sup>	14	29
15→14	133810.844±0.035	51.4	1.434 10 <sup>-04</sup>	15	31
16→15	142730.566±0.045	58.2	1.744 10 <sup>-04</sup>	16	33
17→16	151650.094±0.056	65.5	2.095 10 <sup>-04</sup>	17	35
18→17	160569.416±0.069	73.2	2.491 10 <sup>-04</sup>	18	37
19→18	169488.521±0.083	81.3	2.934 10 <sup>-04</sup>	19	39
20→19	178407.395±0.099	89.9	3.427 10 <sup>-04</sup>	20	41
21→20	187326.026±0.118	98.9	3.971 10 <sup>-04</sup>	21	43
22→21	196244.404±0.138	108.3	4.571 10 <sup>-04</sup>	22	45
23→22	205162.515±0.160	118.2	5.227 10 <sup>-04</sup>	23	47
24→23	214080.348±0.185	128.4	5.944 10 <sup>-04</sup>	24	49
25→24	222997.889±0.211	139.1	6.724 10 <sup>-04</sup>	25	51
26→25	231915.129±0.240	150.3	7.569 10 <sup>-04</sup>	26	53
27→26	240832.053±0.272	161.8	8.482 10 <sup>-04</sup>	27	55
28→27	249748.650±0.306	173.8	9.466 10 <sup>-04</sup>	28	57
29→28	258664.908±0.342	186.2	1.052 10 <sup>-03</sup>	29	59
30→29	267580.815±0.381	199.1	1.166 10 <sup>-03</sup>	30	61